Evolutionary divergence of locomotion in two related vertebrate species

Gokul Rajan, Julie Lafaye, Martin Carbo-Tano, Karine Duroure, Giulia Faini, Dimitrii Tanese, Thomas Panier, Raphaël Candelier, Joerg Henninger, Ralf Britz, et al.

Cell Reports

Evolutionary divergence of locomotion in two related vertebrate species

Graphical abstract

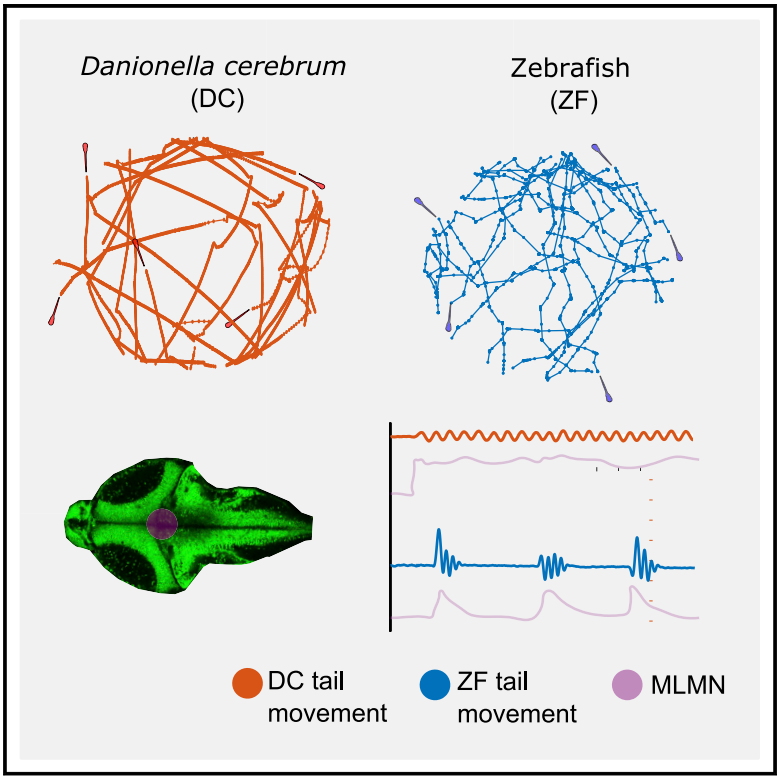

Authors

Gokul Rajan, Julie Lafaye, Giulia Faini, ..., Georges Debregeas, Claire Wyart, Filippo Del Bene

Correspondence

filippo.del-bene@inserm.fr

In brief

Rajan et al. show the divergent swimming patterns employed by two closely related vertebrate species to explore their environment. The authors identify a midbrain nucleus, named mesencephalic locomotion maintenance neurons (MLMNs), to play a significant role in this divergence by (initiating and) prolonging the duration of swim events.

Highlights

- DC executes slower and continuous swimming in contrast to ZF
- DC maintains its heading persistence for a longer time when compared with ZF
- Distribution of functionally important hindbrain neurons is conserved between DC and ZF
- Activation of MLMNs is sufficient to prolong the swimming duration

Rajan et al., 2022, Cell Reports *38*, 110585
March 29, 2022
https://doi.org/10.1016/j.celrep.2022.110585

CellPress

Cell Reports

CellPress
OPEN ACCESS

Report

Evolutionary divergence of locomotion in two related vertebrate species

Gokul Rajan,[1,2] Julie Lafaye,[3,8] Giulia Faini,[1,8] Martin Carbo-Tano,[4] Karine Duroure,[1,2] Dimitrii Tanese,[1] Thomas Panier,[3] Raphaël Candelier,[3] Jörg Henninger,[5] Ralf Britz,[6] Benjamin Judkewitz,[5] Christoph Gebhardt,[2,7] Valentina Emiliani,[1] Georges Debregeas,[3] Claire Wyart,[4] and Filippo Del Bene[1,2,9,*]

[1]Sorbonne Université, INSERM, CNRS, Institut de la Vision, 75012 Paris, France
[2]Institut Curie, PSL Research University, INSERM U934, CNRS UMR3215, Paris, France
[3]Sorbonne Université, CNRS, Institut de Biologie Paris-Seine (IBPS), Laboratoire Jean Perrin (LJP), 75005 Paris, France
[4]Institut du Cerveau (ICM), Sorbonne Universités, UPMC Univ Paris 06 CNRS UMR 7225, Inserm U1127, Hôpital Pitié-Salpêtrière, 75013 Paris, France
[5]Charité-Universitätsmedizin Berlin, Einstein Center for Neurosciences, NeuroCure Cluster of Excellence, 10117 Berlin, Germany
[6]Senckenberg Naturhistorische Sammlungen Dresden, Museum für Zoologie, 01109 Dresden, Germany
[7]Present address: Mortimer B. Zuckerman Mind Brain Behavior Institute, Columbia University, New York, NY 10027, USA
[8]These authors contributed equally
[9]Lead contact
*Correspondence: filippo.del-bene@inserm.fr
https://doi.org/10.1016/j.celrep.2022.110585

SUMMARY

Locomotion exists in diverse forms in nature; however, little is known about how closely related species with similar neuronal circuitry can evolve different navigational strategies to explore their environments. Here, we investigate this question by comparing divergent swimming pattern in larval *Danionella cerebrum* (DC) and zebrafish (ZF). We show that DC displays long continuous swimming events when compared with the short burst-and-glide swimming in ZF. We reveal that mesencephalic locomotion maintenance neurons in the midbrain are sufficient to cause this increased swimming. Moreover, we propose that the availability of dissolved oxygen and timing of swim bladder inflation drive the observed differences in the swim pattern. Our findings uncover the neural substrate underlying the evolutionary divergence of locomotion and its adaptation to their environmental constraints.

INTRODUCTION

Danionella cerebrum (DC) are minute cyprinid fish that show an extreme case of organism-wide developmental truncation or paedomorphosis, which leads to a small adult body size combined with a partially developed cranium without a skull roof. This feature, together with its transparency throughout the adult stages, makes them interesting for functional neuroscience studies allowing the imaging of the entire brain at cellular resolution (Schulze et al., 2018). Due to their high similarity with *D. translucida* (DT), they were misidentified as DT until very recently when they were identified to be a new species of *Danionella* (Britz et al., 2021). Ossification studies in *Danionella* sp. demonstrate that most bones affected by developmental truncation are formed later in the development of ZF (Britz et al., 2009; Conway et al., 2020). Hence, in the early stages of their development, DC and ZF are highly comparable. *Danionella* (DC and DT) and ZF are also found in similar tropical freshwater environments in Asia and are evolutionarily very closely related (Roberts, 1986; Britz et al., 2021; Parichy, 2015). This proximity is an advantage for comparative studies of larval DC and ZF as it provides an opportunity to understand how differences in behaviors can arise from relatively conserved neuronal circuits.

Locomotion is a basic behavior exhibited by most animals and can be reliably quantified and interpreted. Fish can exhibit diverse forms of locomotion using their pectoral, dorsal, caudal, and anal fins (Katz and Hale, 2017). This diversity provides a rich toolkit to dissect and understand the general principles of organization and function of the motor system. ZF exhibits swimming in temporally distinct events called bouts. Each bout consists of a tail burst followed by a glide. Kinematic analysis of swim bouts has produced information on different movement patterns produced by larval ZF. During exploration, forward propulsion is achieved by low-angle slow-swim movements or scoots, along with faster swims called burst swims where large tail amplitudes are used (Budick and O'Malley, 2000).

At the physiological level, calcium imaging in ZF has suggested that the activity of the nucleus of the medial longitudinal fasciculus (nMLF) is associated with swimming activity (Severi et al., 2014). A glutamatergic V2a neuronal population is reported to be associated with initiation of locomotion in ZF (Kimura et al., 2013) and the anterior rhombencephalic turning region is implicated in turning behavior (Dunn et al., 2016). However, the upstream control over the hindbrain nuclei associated with locomotion is not well characterized in ZF. The role of the mesencephalic locomotor region in mammals and lamprey is well established in

modulating the activity of downstream reticulospinal neurons (Ryczko and Dubuc, 2013; Roseberry et al., 2016; Grätsch et al., 2019). The homologous neuronal populations remain uncharacterized in ZF at the moment.

More recently, using unsupervised clustering, Marques et al. (2018) have identified 13 basic swim types that are used in various combinations across different behavioral contexts in ZF. An interesting approach would be to dissect these swim types into their respective neuronal correlates and to investigate how these swim types and their usage across behaviors have diverged over evolution among various danionin larvae with respect to the underlying neuronal correlates. As a first step in this direction, we demonstrate differences in the explorative swimming of DC and ZF despite their evolutionary closeness and investigate the factors, ethological and physiological, underlying this divergence. We used high-speed imaging to characterize the continuous and intermittent swimming patterns executed by DC and ZF, respectively. Using light-sheet imaging and holographic optogenetic stimulation, we identify a neuronal population which can regulate the observed difference in the swimming pattern of the two fish species.

RESULTS

DC larvae exhibit slow and continuous swimming activity

During undulatory swimming, animals experience viscous and inertial forces in the fluid. Based on the body length, the hydrodynamics dictating the swimming also changes (Van Leeuwen et al., 2015; Müller and Van Leeuwen, 2004). However, the body length of larval ZF and DC falls in a similar range of few millimeters, which leads to a transitional flow regime for both (Figures 1A and 1B; size range, 4.1–4.9 mm) (Müller and Van Leeuwen, 2004). To compare the kinematics of their spontaneous swimming, we recorded their movement with a high-speed imaging system. Larval ZF are known to swim in a beat-and-glide pattern wherein a burst of tail activity lasting ~140 ms enables them to swim at high speed and is followed by a passive glide phase (Budick and O'Malley, 2000). In contrast, larval DC do not display distinct bouts but rather move continuously at a low speed with the tail beating for few tens or even hundreds of seconds (Figures 1C, 1D; Videos S1 and S2). To compare the fine swimming kinematics of DC and ZF, we defined kinematic parameters based on half tail beats, a unit common to the swimming pattern of the two species (Figures S1A–S1G). The continuous slow swims of larval DC occur with a smaller half tail beat frequency and a smaller maximum tail angle compared with larval ZF (Figure 1E). In head-embedded preparation, continuous and intermittent swimming patterns were observed as well in larval DC and ZF, respectively (Figure 1F): DC swims for 98.5% of the total recording time compared with only 2% in ZF (Figure 1G). While a head-embedded preparation of ZF is known to show an increase in bout duration (Severi et al., 2014), thereby deviating from the spontaneous swimming kinematics, we inevitably must use a head-embedded preparation for brain imaging studies to restrict movement. Moreover, such an increase in swimming activity in a head-embedded preparation, likely arising due to altered motor feedback to the fish brain, is observed in both DC and ZF, while still preserving the large difference in the total swimming activity between the two species (Figures S1H–S1J).

Escape response is conserved between DC and ZF

To test the ability of larval DC to achieve fast speeds following sensory stimulation, we examined their escape response using tap-induced escape assay (Video S3) (Budick and O'Malley, 2000). Figure 1H shows the striking similarity in the escape response between DC and ZF. Both fish species initiate a fast C-bend followed by a counter bend. DC was found to swim with a lower mean speed and cover a smaller distance during this period compared with ZF (Figures 1I and S1K–S1M). On the other hand, the delay to achieve maximum speed during escape was surprisingly smaller in DC. This faster response may compensate for the relatively lower speed of DC during an escape response (Figure 1I). Our data show that DC are capable of executing fast swims to escape but have evolved a slow and continuous swimming mode during spontaneous exploratory behavior.

Swimming in DC consists of a long ballistic phase

We further investigated how the distinct modes of spontaneous navigation shown by both species may impact their long-term exploratory kinematics. We monitored the swim trajectories of DC and ZF in a 60-mm-diameter Petri dishes as shown in Figures 2 A and 2B. We then computed the mean square displacement (MSD) that quantifies the area explored by the animal over a given period of time (Figure 2C). Surprisingly, although the DC mean forward velocity is significantly lower than ZF, the MSDs are comparable. This can be understood by considering differences in heading persistence in both species. At short timescale, the larvae tend to swim in straight lines such that their trajectories can be considered ballistic (heading straight in the same direction). On longer timescales, reorientation events cumulatively randomize the heading direction and the dynamics becomes diffusive-like. The ballistic-to-diffusive transition time can be estimated by computing the decorrelation in heading direction, as shown in Figure 2D. These graphs reveal a faster randomization of heading direction in ZF compared with DC. In ZF, the decorrelation function R(t) drops down to 0.3 in ~1 s, i.e., the typical inter-bout interval, then decays to 0 in 6–7 s. In DC, R(t) shows a small initial drop (down to 0.8) then slowly decays to 0 over the next ~8 s. The small initial decay in the first ~0.5 s can be interpreted as reflecting the short timescale fluctuations in heading direction during run periods. The further slow decorrelation in turn results from the successive reorientation events that separate the periods of straight swimming, a process reminiscent of the classical run-and-tumble mechanism of motile bacteria (Berg and Brown, 1972; Watari and Larson, 2010). The timescale of this slow decay is expected to be controlled by the interval between successive reorientation events, which is of order of 5–10 s.

To quantitatively assess the relative contribution of the ballistic versus diffusive components of the MSD over time, we estimated the former as:

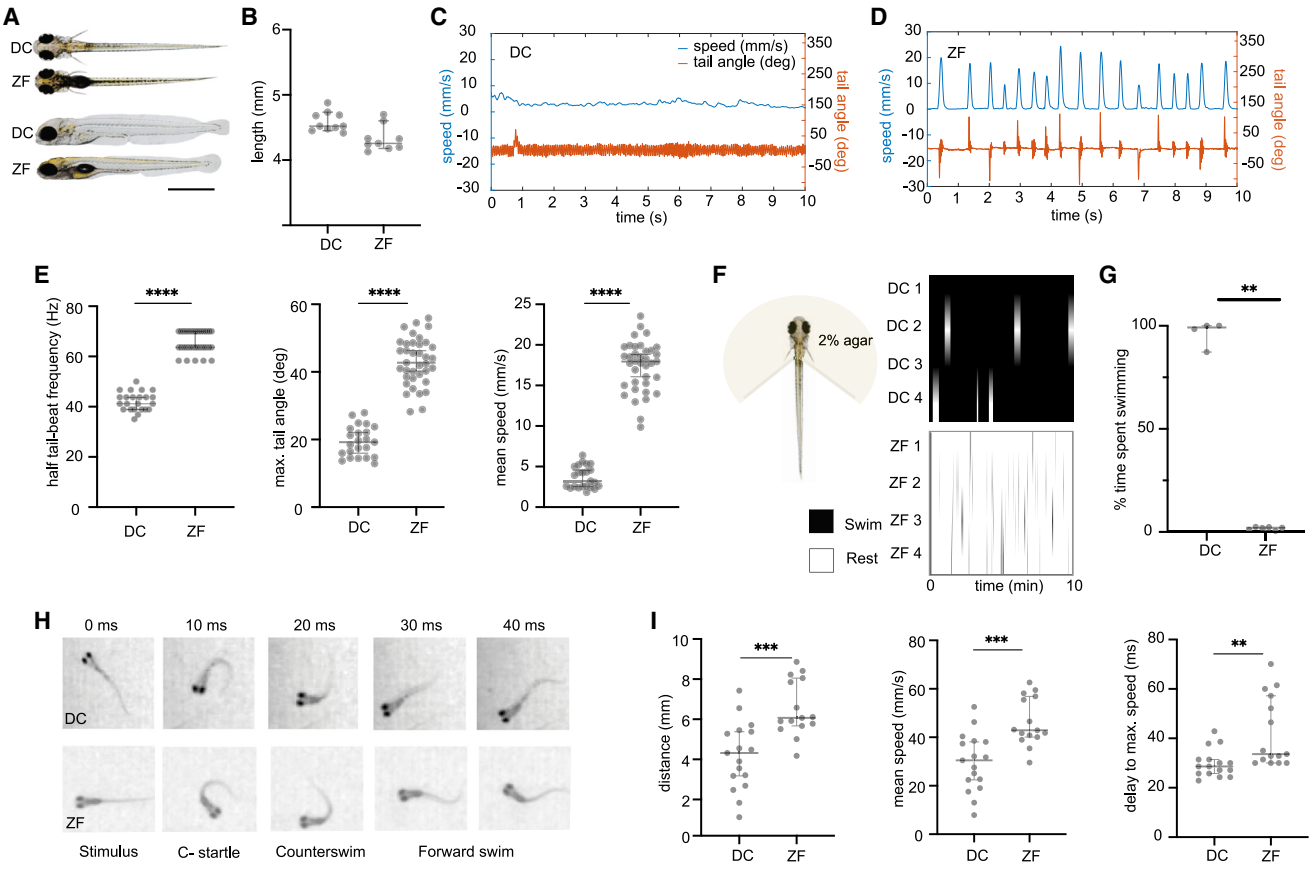

Figure 1. Kinematics of spontaneous swimming, head-embedded swimming, and escape response in DC and ZF

Larval DC and ZF measure similar in size at 5 dpf.

(A) A dorsal and lateral view of DC and ZF at 5 dpf is shown.

(B) Measurement of body length in 5 dpf DC and ZF falls in a range of 4.1–4.9 mm. N = 10 DC; N = 9 ZF.

(C and D) A comparison of swimming patterns in 6 dpf DC and ZF. It demonstrates the continuous swimming pattern in DC with lower speed (cyan) and smaller tail angle (orange) when compared with the faster discrete swimming in ZF.

(E) Swimming kinematics of DC and ZF in a spontaneous swimming assay. DC utilizes lower half tail beat frequency (Hz) and lower maximum tail angles (degrees) to achieve swimming at lower speeds (mm/s) when compared with ZF (N = 23 DC, n = 494,628 half tail beats and N = 37 ZF, n = 202,176 half tail beats).

(F) Tail movements in head-embedded preparations depicted in raster plots illustrate the prolonged swims of DC (top) compared with the short bouts of ZF (bottom).

(G) The fraction of time spent actively swimming (percent of total acquisition time) is higher in DC compared with ZF (N = 5 DC and N = 6 ZF).

(H) Qualitatively, the escape response after a tap stimulus is highly similar between DC and ZF. The images were acquired at 100 Hz.

(I) Although DC covers a shorter distance at a lower mean speed, the time to achieve the maximum speed is lower in DC compared with ZF (DC, N = 19 fish, n = 141 events; ZF, N = 15 fish, n = 159 events). **p < 0.01, ***p = 0.001, ****p < 0.0001; Mann-Whitney test. All error bars show 95% confidence interval. See also Figure S1.

$$MSD_{bal}(t) = \left\langle \left[\int_{t_0}^{t_0+t} v * R(t' - t_0).\, dt' \right]^2 \right\rangle_{t_0},$$

where v is the mean instantaneous velocity. As expected, for a purely ballistic process, R = 1 and $MSD_{bal} = (vt)^2$, whereas, for a purely diffusive process, R = 0 and $MSD_{bal} = 0$. For DC, this quantity correctly captures the MSD up to ~6 s (Figure 2C), indicating that the ballistic component is dominant over this long initial period. In contrast, for ZF, the MSD departs from the ballistic component from 1 s onward, i.e., after one to two bouts. In summary, our analysis shows that the pattern of navigation adopted by DC yields longer heading persistence, which almost exactly compensates for its intrinsically lower swimming speed and results in comparable long-term spatial explorations.

Different swim patterns follow adaptations to oxygen availability and swim bladder development

We next asked what selective environmental and physiological pressures might have led to the differing swimming patterns. At the environmental level, we explored the role of dissolved oxygen on these differences. During our field study in Myanmar, we found that adult DC were most

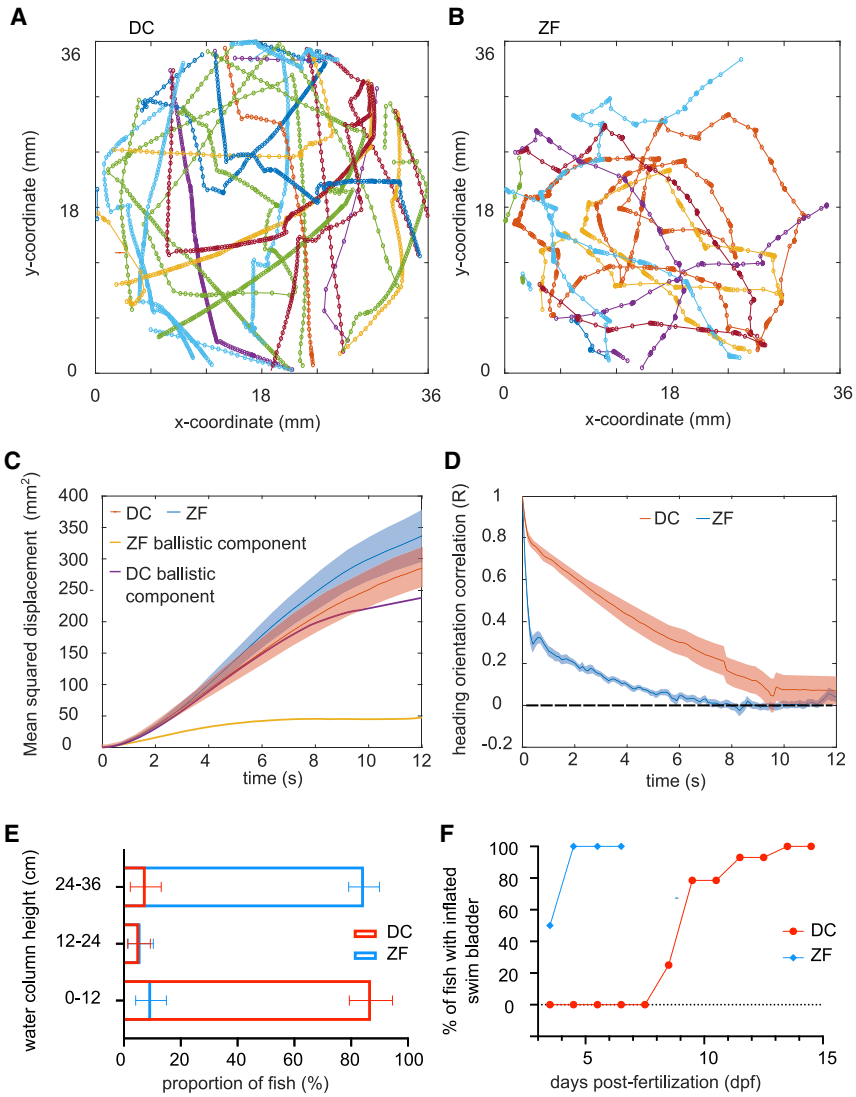

Figure 2. Long-term exploratory kinematics of DC and ZF

(A and B) A few tens of swim trajectories depicted in different colors from a single DC and ZF larva, respectively.

(C) Mean squared displacement (MSD) in DC and ZF over time. The MSD over time for the ballistic component of DC and ZF is also overlapped on the plot. N = 23 DT and 37 ZF. The error bars show SEM.

(D) Decorrelation in heading persistence over time. R = 1 indicates a perfect persistence in head direction, whereas R = 0 corresponds to a dull randomization. In ZF, R drops rapidly, whereas this drop happens over longer period of time in DC. Hence, exploratory swimming in DC has a longer ballistic phase. N = 23 DT and 37 ZF. The error bars show SEM.

(E) DC larvae occupy the bottom of the water column, whereas ZF larvae occupy the top. N = ~30 fish and n = 10 readings in 3 replicates for each fish species. The error bars show 95% confidence interval.

(F) Swim bladder inflation in ZF occurs earlier than in DC. The inflation of swim bladder in ZF occurs by ~ 4–5 dpf, whereas DC inflates their swim bladder between ~10 and ~15 dpf. Sampled from a growing population of approximately N = 30 DC and 30 ZF. See also Figures S2.

abundant at the lower water levels of a small stream at ~50 cm, characterized by lower oxygen levels compared with the surface (O_2 = 8.75 mg/L at the surface; O_2 = 3.5 mg/L at 50 cm; O_2 = 2.8 mg/L at 80 cm) (Figure S2A) (Britz et al., 2021). In contrast, adult ZF are reported in waters with variable DO concentration with a median of 5.55 ± 1.64 mg/L, but this lacks information on the depth at which it was recorded (Shukla and Bhat, 2017). In the laboratory, we tested the occupancy of larval DC and ZF in a tall water column of 36 cm height. Larval DC were found to occupy the lower zone of the water column whereas larval ZF were found in the upper zone of the water column (Figure 2E). This is consistent with previous observations that ZF adults spawn in very shallow environments while adult DC spawn in the narrow spaces in the bottom of the river bed (Parichy, 2015; Schulze et al., 2018). As we have seen, upper layers of a water column in the wild are richer in dissolved oxygen (DO) when compared with the bottom layers (Boehrer and Schultze, 2008; Davis, 1975). Hence, the apparent preference of DC for deeper water would accompany a lower availability of DO in the wild. This lower DO availability would have consequences on swimming at two levels: during locomotion and at rest. During locomotion, a lower DO would act as a constraint to the maximum swimming speed that can be achieved by an animal (Figure S2B) (Bagatto et al., 2001). At rest, it has been shown, both experimentally and analytically, that increased body movements with reduced stationary periods would be beneficial for larval fish in a low DO environment to be able to replenish DO in its immediate surrounding (Figure S2C) (Green et al., 2011; Weihs, 1980) .

At the physiological level, we propose that a difference in the timing of swim bladder inflation in DC and ZF might have an important role in the observed differences in the swimming pattern. We observed inflation of swim bladder in ZF by ~4–5 dpf, whereas in the DC population this occurred later, between 10 and 15 dpf (Figures 2F and S2D). Without a swim bladder to regulate its buoyancy, a fish might need to swim more continuously and exert a downward force to actively maintain its position in the water column (Denton and Marshall, 1958). Consistent with this hypothesis, 5 dpf ZF larvae without an inflated swim bladder had a smaller inter-bout interval of 242.86 ms when compared with the group with an inflated swim bladder (499.29 ms) (Figures S2E–S2H).

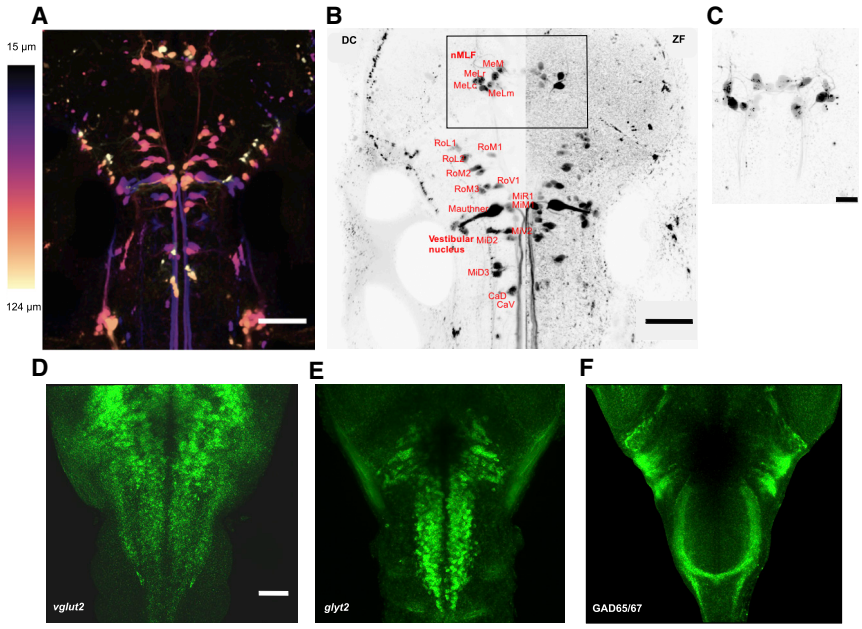

Figure 3. Distribution of reticulospinal neurons and excitatory and inhibitory neuronal cell types in the hindbrain of DC and ZF

(A) Distribution of reticulospinal (RS) neurons in the brainstem of DC. Maximum intensity is color coded for depth. Scale bar, 100 µm.

(B) Comparison of RS neurons in DC and ZF. A cell-to-cell comparison of RS neurons in a maximum intensity projection of RS neurons in DC and ZF. The RS neurons in DC are annotated based on the description of RS neurons in ZF (Kimmel et al., 1982; Orger et al., 2008). A high degree of conservation is observed. Scale bar, 100 µm.

(C) A closer look at the rectangular region of interest (ROI) from (B) in another DC fish. Maximum intensity projection of the nucleus of the medial longitudinal fasciculus (nMLF) in another DC fish is shown. Contralateral dendritic projections are observed in DC as noted in ZF (Kimmel et al., 1982). Scale bar, 30 µm.

(D–F) Distribution of (D) glutamatergic, (E) glycinergic, and (F) GABAergic neurons in the hindbrain of DC. Performed using *in situ* hybridization (ISH) and immunohistochemistry (IHC). Rostrocaudally running striped pattern of these neuronal types is observed in DC as noted in ZF before (Higashijima et al., 2004). Anti-*vglut2a* + anti-*vglut2b* ISH and anti-*glyt2* ISH in (D and E), respectively. Anti-GAD65/67 IHC in (F). All images are a maximum intensity projection. Scale bar, 50 µm. See also Figure S3.

Distribution of major neuronal populations in the hindbrain is conserved between DC and ZF

To determine the cellular underpinnings of the difference in swimming modes (continuous versus discrete) in the two species, we first investigated the organization of neuronal populations in DC. We initially examined reticulospinal neurons in the brainstem as these neurons projecting from hindbrain to spinal cord are known to play a role in locomotion control in all vertebrates (Bouvier et al., 2015; Juvin et al., 2016; Kimura et al., 2013). We identified numerous cells of the mesencephalic nucleus of the medial longitudinal fascicle (nucMLF/nMLF), the rhombocephalic reticular formation (nucRE), and the rhombocephalic vestibular nucleus (nucVE), whose location of soma and morphology showed a high homology with cells described previously in ZF (Figure 3B) For instance, we observed dendrites crossing the midline from the MeM cells (of nMLF) in DC as described previously in ZF (Figure 3C) (Kimmel et al., 1982; Orger et al., 2008). Next, we investigated the distribution of excitatory (glutamatergic) and inhibitory (glycinergic and GABAergic) neurons in the hindbrain. In ZF, these populations are described to be spatially organized in distinct stripes ordered according to their developmental age and neurotransmitter identity (Higashijima et al., 2004; Kinkhabwalaa et al., 2011; Koyama et al., 2011). Consistent with this arrangement, the distribution of excitatory and inhibitory neurons in DC hindbrain also forms rostro-caudally running stripes (Figures 3D and 3F; and cross-section in Figures S3A–S3C).

Different neurons correlate with maintenance and termination of swimming activity

To identify functional differences in neuronal activation during spontaneous locomotion, we investigated the recruitment of neurons throughout the brain using whole-brain calcium imaging in larval DC and ZF. We generated a transgenic line *Tg(elavl3:H2B-GCaMP6s)* in DC where the calcium indicator, GCaMP6s, was nuclear-targeted and expressed under a pan-neuronal promoter as previously done in ZF (Figures S3D and S3E) (Chen et al., 2013). Using light-sheet microscopy, we acquired a brain stack of ~200 µm depth at ~1 volume per second while simultaneously recording the tail motion in a head-embedded preparation (Figures S3F and S3G). To identify the supraspinal neurons recruited during spontaneous locomotion in the two species, we performed a regression analysis on the fluorescence signal of single neurons using regressors representing swimming and termination of swimming (Figure S3H).

This approach, based on correlation, revealed neurons in the hindbrain of DC reliably recruited during the termination of swimming and that may therefore be referred as putative "stop neurons" (Figures 4A and 4B). With respect to initiation and maintenance of swimming activity, we identified putative locomotor regions in the brain of larval DC and ZF that were highly correlated with the swim events (Figures 4C, 4D, and S3D–S3J). The neuronal activity in these nuclei correlated with the duration of swim events in DC and ZF (Figure 4E), suggesting a role in the start and/or maintenance of swimming. Among these regions, we identified a strongly correlated midbrain nucleus referred to here as the mesencephalic locomotion maintenance neurons (MLMNs).

Optogenetic activation of MLMNs in ZF leads to increased swimming

To dissect the role of MLMNs in maintenance of the long swim events, we carried out optogenetic stimulation in ZF *Tg(elavl3:CoChR-eGFP)*, which express the opsin CoChR under a pan-neuronal promoter. We targeted MLMNs using 2-photon

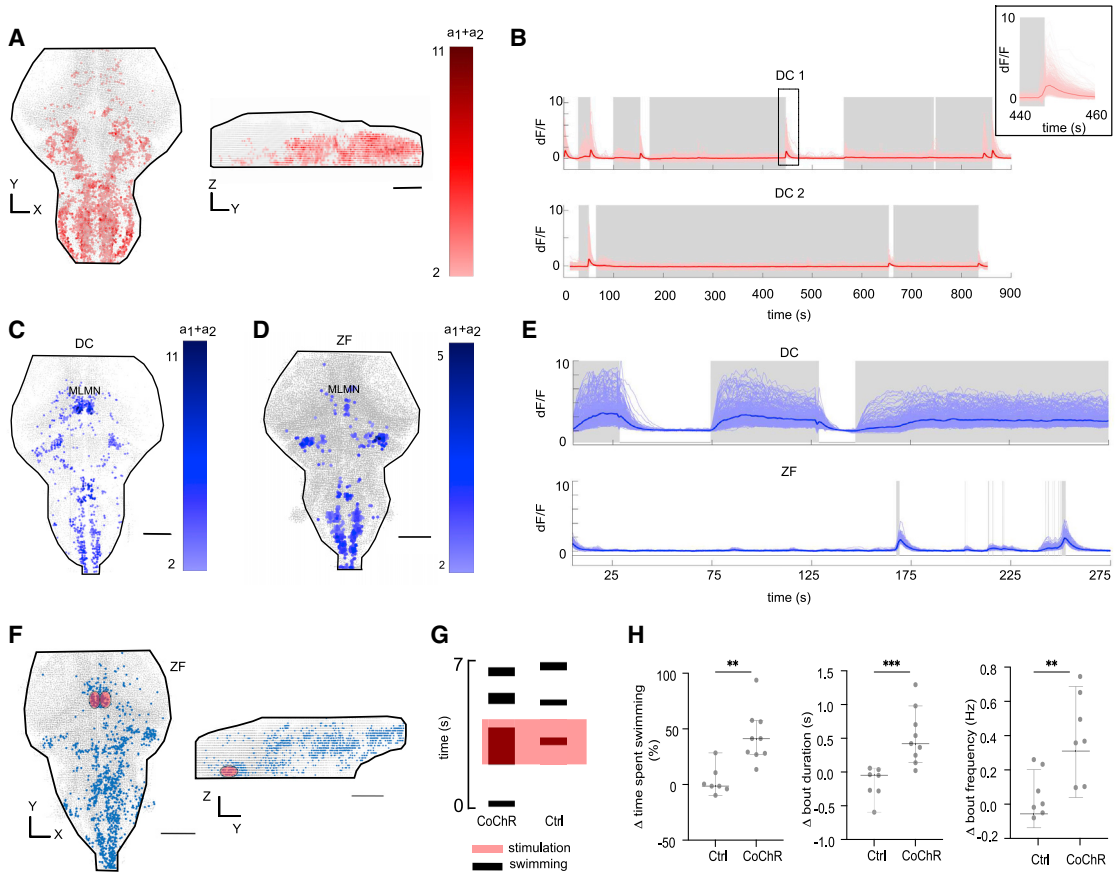

Figure 4. Neurons correlated with termination of swimming (in DC) and swimming (in DC and ZF); and holographic stimulation of the identified mesencephalic locomotion maintenance neurons (MLMNs)

(A) Representative images of stop cells (in red) identified in the DC hindbrain (N = 3 fish).

(B) The activity of the identified stop neurons (in red) with respect to swimming activity (in gray). The inset shows a magnified region around a swim termination event.

(C and D) A representative figure of a maximum projection of neuronal correlates of swimming (in blue) identified in the DC and ZF brain, respectively. The nuclei correlated with swimming appear to be conserved between DC (N = 4 fish) and ZF (N = 4 fish). The MLMN population is labeled.

(E) Neuronal activity of all the swimming correlated neurons in DC compared with the corresponding neurons' activity in a ZF for a duration of 300 s. The activity in the conserved nuclei in DC is sustained for long durations unlike ZF, correlating with their long swim events. The gray shaded regions represent active swimming.

(F) The region of interest (ROI) for holographic optogenetic stimulation is illustrated. MLMN population described in (C and D) was first anatomically located under a 2-photon microscope using expression of CoChR-GFP (in test) or GCaMP6 (in control) as the guidance cue. A holographic stimulation protocol was then employed in this ROI (see Figures S4A–S4C).

(G) The result of the stimulation in a CoChR and Ctrl fish. Swimming activity in CoChR fish is increased during the holographic stimulation.

(H) Change in total swimming time, bout duration, and bout frequency during optogenetic stimulation. The time spent swimming is prolonged in test fish by the optogenetic stimulation; this increase is caused by both, an increased recruitment of bouts and an increase in the duration of the bouts. N = 7 Ctrl ZF and 9 CoChR ZF. **$p < 0.01$, ***$p = 0.001$; Mann-Whitney test. All error bars show 95% confidence interval. Scale bars, 100 μm. See also Figures S3 and S4.

holographic stimulation with temporal focusing (Figures 4F and S4A–S4C) (Chen et al., 2018) and observed a reliable increase in swimming following the stimulation (Figures 4G, 4H; Video S4). MLMN stimulation led to an increase in the mean duration of bouts and an increase in the frequency of bouts (Figure 4H), indicating an important role for MLMNs in the maintenance of long swim events. The recruitment of swimming on mere stimulation of MLMNs alone also suggests that this neuronal population also comprises some initiation neurons. A reduction in the duration of swim events and overall swimming in spinalized preparation of DC further corroborates the necessity of this supraspinal signal to maintain the continuous swimming in DC (Figures S4D–S4F).

DISCUSSION

We show that the two species achieve their different swimming patterns by exploiting different fine kinematics. Despite this, their long-term spatial exploration appears similar due to the underlying difference in the reorientation kinematics wherein DC executes long ballistic movements. We have proposed that the adaptation to availability of dissolved oxygen and different timing

of swim bladder inflation are the reasons underlying the evolution of difference in swimming pattern. As we observed, 5dpf ZF larvae swim with shorter inter-bout intervals in the absence of an inflated swim bladder. It is this adaptive decrease in inter-bout interval that can be strongly selected for over the evolutionary time course in larvae without an inflated swim bladder. However, it is important to note that the delayed inflation of swim bladder alone cannot explain the difference observed in the swimming pattern. Indeed, we evaluated swimming in DC and ZF larvae at 15 dpf when all the animals have inflated swim bladder. Although a decrease was seen in the proportion of time spent swimming in 15 dpf DC when compared with 6 dpf DC, this value remained much higher compared with ZF at 6 and 15 dpf (Figure S2D). Altogether, our data show that the slow and continuous swimming pattern of DC might be a result of adaptation to a combination of factors, which include lower availability of dissolved oxygen and delayed inflation of the swim bladder. Of course, many animals thrive in deep sea environments with extremely low oxygen levels but this might be dependent on a number of physiological adaptations selected over a very long evolutionary time, which have promoted lower oxygen consumption (Childress and Seibel, 1997). In closely related freshwater species as analyzed here, we suggest that more subtle behavioral adaptations, such as a difference in swimming pattern, may have been selected.

We show nearly identical distribution of reticulospinal neurons and other neuronal makers, which points to a closely conserved bauplan of the hindbrain locomotor control region. However, homologous neurons could have different functions, as shown for neurons involved in feeding behaviors in nematodes (Newcomb et al., 2012). Functionally, we identified stop and maintenance neuronal populations in the DC brain that correlate with termination and maintenance of swimming activity, respectively. Stop neurons responsible for termination of locomotion have been reported in other vertebrates, such as tadpole, lamprey, and mice (Bouvier et al., 2015; Juvin et al., 2016; Perrins et al., 2002), but the short swim events of ZF make it difficult to survey such functional cell types at the whole-brain scale. DC's long swim events offered a unique opportunity to resolve neurons active at the termination of swimming, and pinpoint motor areas recruited for movement termination. This demonstrates another benefit of employing related animal species in functional studies in addition to their obvious use in understanding evolution of neuronal circuits.

Our work identified a neuronal population called MLMNs, the activity of which correlates with the swimming activity. We decided to focus on this region as the most interesting candidate to sustain the long swim events in DC as previous work in ZF has revealed an anatomically corresponding region suggested to comprise nMLF as well as other glutamatergic neurons that are implicated in swimming activity (Abdelfattah et al., 2019; Dunn et al., 2016; Severi et al., 2014). The nMLF specifically is known to have projections to the caudal hindbrain and spinal cord and plays an important role in locomotor control (Severi et al., 2014; Thiele et al., 2014). A gain-of-function experiment using optogenetic activation in ZF was performed for causal validation as suitable transgenic lines only exist in ZF. We show that optogenetic activation of MLMNs was sufficient to cause longer swimming events in ZF. However, the discrete swimming patterns of ZF was still maintained with longer bout lengths despite the sustained stimulation of MLMNs. This suggests that the signal for discrete swimming in ZF is at least partly embedded in a downstream locomotor control circuit, possibly in the spinal cord as previously observed in spinalized ZF preparations deprived of supraspinal inputs (Wiggin et al., 2012; McDearmid and Drapeau, 2006). It is to be noted that, while spinal CPG in DC could also have co-evolved to some extent to produce longer swim periods, the swim events appeared short-lasting and more frequent with an overall decrease in swimming activity (a more intermittent swimming pattern like ZF) in a spinalized preparation of DC. However, the DC-like swimming pattern could be recovered by application of a pharmacological excitation to the preparation (Figures S4D–S4F). This corroborates the necessity of an excitatory supraspinal signal to generate the observed swimming pattern in DC. The long-lasting neuronal activity that we observe in MLMNs of DC could be linked to intrinsic membrane or network properties of the identified neurons (Antri et al., 2009; Li et al., 2006). Overall, our work shows how this comparative approach, using whole-brain imaging data from related species that show discrete divergent behaviors, can identify functionally relevant population.

In conclusion, using two closely related fish species, we show that two anatomically similar brains with conserved features can produce different behavioral outputs based on functional differences in a subset of neurons called MLMNs. We also suggest selective pressures that could have led to the divergence of the swimming pattern. This lays the foundation for future work to directly compare neuronal circuits and behaviors in vertebrate species, applying an approach that has been very successfully used in various invertebrate studies (Newcomb et al., 2012; Seeholzer et al., 2018). This is particularly interesting to perform in danionin fish as many related species are known and can be raised in a laboratory setting. With the ability to assign behavioral modules to their corresponding genetic and neuronal circuit components in ZF (and other danionins), our work provides a powerful approach in comparative neuroethology to investigate evolution of behaviors and neuronal circuits in vertebrates.

Limitations of the study

In this study, the role of MLMNs could not be verified directly in DC as relevant transgenic lines do not yet exist to test this in a non-invasive manner. The identification of putative ''stop neurons'' based on correlation will also benefit from a cross-species brain registration and experimental test of causality in the future. Moreover, in the current work, we have not identified the cellular changes which lead to this difference in the firing properties of the MLMNs in the two species. Future work can ascertain if intrinsic membrane properties, network property, or neuromodulatory signals play a role in this.

STAR★METHODS

Detailed methods are provided in the online version of this paper and include the following:

- KEY RESOURCES TABLE
- RESOURCE AVAILABILITY
  - Lead contact

- Materials availability
- Data and code availability
- EXPERIMENTAL MODEL AND SUBJECT DETAILS
- METHOD DETAILS
  - Free-swimming behavioral acquisition, fish tracking and tail segmentation
  - Analysis pipeline for free-swim data
  - Half beat based kinematics in ZF and DC
  - Head-embedded swimming
  - Tap-induced escape behavior
  - Mean squared displacement (MSD) and reorientation analysis
  - Quantification of depth preference
  - Quantification of body length and swim bladder inflation
  - Quantification of influence of swim bladder on swimming kinematics in ZF
  - Whole-mount *in-situ* hybridization (ISH)
  - Vibratome section
  - Whole-mount fluorescence *in-situ* hybridizations (FISH)
  - Immuno-histochemistry
  - Confocal imaging of the whole brain FISH/IHC samples
  - Retrograde labelling of reticulospinal (RS) neurons
  - Motor activity in spinalized preparation of DC
  - Generation of pan-neuronal calcium sensor *Tg(elavl3-H2B:GCaMP6s)* line
  - Light sheet microcopy
  - Image processing and analysis pipeline for whole-brain light-sheet data
  - Brain registration
  - Optogenetic stimulation
- QUANTIFICATION AND STATISTICAL ANALYSIS
  - Behavior data
  - Light-sheet imaging data

SUPPLEMENTAL INFORMATION

Supplemental information can be found online at https://doi.org/10.1016/j.celrep.2022.110585.

ACKNOWLEDGMENTS

We would like to thank Mykola Kadobianskyi for providing us with an early access to the *Danionella cerebrum* genome. Thanks to Adrien Jouary and Michael Orger for sharing their expertise in animal tracking and Roshan Jain for helpful discussion. G.R. was supported by a European Union's Horizon 2020 research and innovation program under the Marie Skłodowska-Curie grant agreement no. 666003, a Fondation pour le Recherche Medicale (FRM) fourth year doctoral fellowship and a Sorbonne University Postdoctoral Fellowship. Work in the laboratory of F.D.B. was supported by ANR-18-CE16 "iReelAx," UNADEV in partnership with ITMO NNP/AVIESAN (National Alliance for Life Sciences and Health), the Fondation Simone and Cino del Duca, and the Program Investissements d'Avenir IHU FOReSIGHT (ANR-18-IAHU-01). B.J. acknowledges support by the German Research Foundation (DFG, project EXC-2049-390688087 and project 432195732), the Einstein Foundation (EPP-2017-413), the European Research Council (ERC-2016-StG-714560) and the Alfried Krupp Foundation. C.G. was supported by an EMBO Short-term Fellowship, an Institut Curie Postdoctoral Fellowship and an FRM Postdoctoral Fellowship. G.D. was supported by H2020 European Research Council (71598).

AUTHOR CONTRIBUTIONS

G.R. and F.D.B. conceived the project with inputs from C.W., G.D., and C.G. G.R. designed all the experiments, developed the behavior rig and transgenic fish, and performed all the experiments and analysis unless otherwise specified. J.L. performed the analysis of the whole-brain data with inputs from G.R. under the supervision of G.D. M.C.-T. and G.R. performed the backfill experiments under the supervision of C.W. K.D. and G.R. performed the other anatomical experiments. D.T. and G.F. performed the optogenetic experiment and analysis under the supervision of V.E. G.F. performed spinalization experiments and analyzed the results. T.P. and R.C. built the light-sheet imaging rig. J.H., B.J., and R.B. obtained data from the field study. F.D.B. and C.G. supervised G.R. G.D. wrote the MSD/reorientation analysis script. The manuscript was written by G.R. and F.D.B. with inputs from other authors. All authors read and approved the final manuscript.

DECLARATION OF INTERESTS

The authors declare no competing interests.

Received: May 12, 2021
Revised: December 15, 2021
Accepted: March 8, 2022
Published: March 29, 2022

REFERENCES

Abdelfattah, A.S., Kawashima, T., Singh, A., Novak, O., Liu, H., Shuai, Y., Huang, Y.C., Campagnola, L., Seeman, S.C., Yu, J., et al. (2019). Bright and photostable chemigenetic indicators for extended in vivo voltage imaging. Science *365*, 699–704.

Accanto, N., Molinier, C., Tanese, D., Ronzitti, E., Newman, Z.L., Wyart, C., Isacoff, E., Papagiakoumou, E., and Emiliani, V. (2018). Multiplexed temporally focused light shaping for high-resolution multi-cell targeting. Optica *5*, 1478–1491. https://doi.org/10.1364/OPTICA.5.001478.

Antri, M., Fénelon, K., and Dubuc, R. (2009). The contribution of synaptic inputs to sustained depolarizations in reticulospinal neurons. J. Neurosci. *29*, 1140–1151.

Bagatto, B., Pelster, B., and Burggren, W.W. (2001). Growth and metabolism of larval zebrafish: effects of swim training. J. Exp. Biol. *204*, 4335–4343.

Berg, H.C., and Brown, D.A. (1972). Chemotaxis in *Escherichia coli* analysed by three-dimensional tracking. Nature *239*, 500–504.

Boehrer, B., and Schultze, M. (2008). Stratification of lakes. Rev. Geophys. *46*, 1–27.

Bouvier, J., Caggiano, V., Leiras, R., Balueva, K., Fuchs, A., and Correspondence, O.K. (2015). Descending command neurons in the brainstem that halt locomotion. Cell *163*, 1191–1203.

Britz, R., Conway, K.W., and Rüber, L. (2009). Spectacular morphological novelty in a miniature cyprinid fish, *Danionella dracula* n. sp. Proc. Biol. Sci. *276*, 2179–2186.

Britz, R., Conway, K.W., and Rüber, L. (2021). The emerging vertebrate model species for neurophysiological studies is *Danionella cerebrum*, new species (Teleostei: cyprinidae). Sci. Rep. *11*, 18942.

Budick, S.A., and O'Malley, D.M. (2000). Locomotion of larval zebrafish. J. Exp. Biol. *203*, 2565–2579.

Chen, I.W., Papagiakoumou, E., and Emiliani, V. (2018). Towards circuit optogenetics. Curr. Opin. Neurobiol. *50*, 179–189.

Chen, T.W., Wardill, T.J., Sun, Y., Pulver, S.R., Renninger, S.L., Baohan, A., Schreiter, E.R., Kerr, R.A., Orger, M.B., Jayaraman, V., et al. (2013). Ultrasensitive fluorescent proteins for imaging neuronal activity. Nature *499*, 295–300.

Childress, J.J., and Seibel, A.B. (1997). Life at Stable low oxygen levels: adaptations of animals to oceanic oxygen minimum layers. J. Exp. Biol. *201*, 1223–1232.

Conway, K.W., Kubicek, K.M., and Britz, R. (2020). Extreme evolutionary shifts in developmental timing establish the miniature *Danionella* as a novel model in the neurosciences. Dev. Dyn. *250*, 601–611.

Davis, J.C. (1975). Minimal dissolved oxygen requirements of aquatic life with emphasis on Canadian species: a review. J. Fish. Res. Board Can. *32*, 2295–2332.

Denton, E.J., and Marshall, N.B. (1958). The buoyancy of bathypelagic fishes without a gas-filled swimbladder. J. Mar. Biol. Assoc. U. K. *37*, 753–767.

Dunn, T.W., Mu, Y., Narayan, S., Randlett, O., Naumann, E.A., Yang, C.T., Schier, A.F., Freeman, J., Engert, F., and Ahrens, M.B. (2016). Brain-wide mapping of neural activity controlling zebrafish exploratory locomotion. Elife *5*, 1–29.

Freeman, J., Vladimirov, N., Kawashima, T., Mu, Y., Sofroniew, N.J., Bennett, D.V., Rosen, J., Yang, C.T., Looger, L.L., and Ahrens, M.B. (2014). Mapping. brain activity at scale with cluster computing. Nat Methods *11*, 941–950. https://doi.org/10.1038/nmeth.3041.

Grätsch, S., Auclair, F., Demers, O., Auguste, E., Hanna, A., Büschges, A., and Dubuc, R. (2019). A brainstem neural substrate for stopping locomotion. J. Neurosci. *39*, 1044–1057.

Green, M.H., Ho, R.K., and Hale, M.E. (2011). Movement and function of the pectoral fins of the larval zebrafish (Danio rerio) during slow swimming. J. Exp. Biol. *214*, 3111–3123.

Higashijima, S.I., Schaefer, M., and Fetcho, J.R. (2004). Neurotransmitter properties of spinal interneurons in embryonic and larval zebrafish. J. Comp. Neurol. *480*, 19–37.

Juvin, L., Grätsch, S., Trillaud-Doppia, E., Gariépy, J.F., Büschges, A., and Dubuc, R. (2016). A specific population of reticulospinal neurons controls the termination of locomotion. Cell Rep. *15*, 2377–2386.

Kadobianskyi, M., Schulze, L., Schuelke, M., and Judkewitz, B. (2019). Hybrid genome assembly and annotation of *Danionella translucida*. Sci Data *6*, 1–7. https://doi.org/10.1038/s41597-019-0161-z.

Katz, P.S., and Hale, M.E. (2017). Evolution of Motor Systems. Neurobiology of Motor Control: Fundamental Concepts and New Directions (USA: John Wiley & Sons, Inc.), pp. 135–176.

Kimmel, C.B., Powell, S.L., and Metcalfe, W.K. (1982). Brain neurons which project to the spinal cord in young larvae of the zebrafish. J. Comp. Neurol. *205*, 112–127.

Kimura, Y., Satou, C., Fujioka, S., Shoji, W., Umeda, K., Ishizuka, T., Yawo, H., and Higashijima, S. (2013). Hindbrain V2a neurons in the excitation of spinal locomotor circuits during zebrafish swimming. Curr. Biol. *23*, 843–849.

Kinkhabwalaa, A., Riley, M., Koyama, M., Monen, J., Satou, C., Kimura, Y., Higashijima, S.I., and Fetcho, J. (2011). A structural and functional ground plan for neurons in the hindbrain of zebrafish. Proc. Natl. Acad. Sci. U S A. *108*, 1164–1169.

Koyama, M., Kinkhabwala, A., Satou, C., Higashijima, S.I., and Fetcho, J. (2011). Mapping a sensory-motor network onto a structural and functional ground plan in the hindbrain. Proc. Natl. Acad. Sci. U S A. *108*, 1170–1175.

Thisse, C., and Thisse, B. (2008). High-resolution in situ hybridization to whole-mount zebrafish embryos. Nat Protoc *3*, 59–69. https://doi.org/10.1038/nprot.2007.514.

Van Leeuwen, J.L., Voesenek, C.J., and Müller, U.K. (2015). How body torque and Strouhal number change with swimming speed and developmental stage in larval zebrafish. J. R. Soc. Interf. *12*, 0479.

Li, W.C., Soffe, S.R., Wolf, E., and Roberts, A. (2006). Persistent responses to brief stimuli: feedback excitation among brainstem neurons. J. Neurosci. *26*, 4026–4035.

Marques, J.C., Lackner, S., Félix, R., and Orger, M.B. (2018). Structure of the zebrafish locomotor repertoire revealed with unsupervised behavioral clustering. Curr. Biol. *28*, 181–195.e5.

McDearmid, J.R., and Drapeau, P. (2006). Rhythmic motor activity evoked by NMDA in the spinal zebrafish larva. J. Neurophysiol. *95*, 401–417.

Migault, G., van der Plas, T.L., Trentesaux, H., Panier, T., Candelier, R.L., Proville, R., Englitz, B., Debregeas, G., and Bormuth, V. (2018). Whole-Brain Calcium Imaging during Physiological Vestibular Stimulation in Larval Zebrafish. Curr Biol *28*, 3723–3735. https://doi.org/10.1016/j.cub.2018.10.017.

Müller, U.K., and Van Leeuwen, J.L. (2004). Swimming of larval zebrafish: ontogeny of body waves and implications for locomotory development. J. Exp. Biol. *207*, 853–868.

Newcomb, J.M., Sakurai, A., Lillvis, J.L., Gunaratne, C.A., and Katz, P.S. (2012). Homology and homoplasy of swimming behaviors and neural circuits in the Nudipleura (Mollusca, Gastropoda, Opisthobranchia). Proc. Natl. Acad. Sci. U S A. *109*, 10669–10676.

Orger, M.B., Kampff, A.R., Severi, K.E., Bollmann, J.H., and Engert, F. (2008). Control of visually guided behavior by distinct populations of spinal projection neurons. Nat Neurosci. *11*, 327–333.

Parichy, D.M. (2015). Advancing biology through a deeper understanding of zebrafish ecology and evolution. Elife *4*, e05635.

Perrins, R., Walford, A., and Roberts, A. (2002). Sensory activation and role of inhibitory reticulospinal neurons that stop swimming in hatchling frog tadpoles. J. Neurosci. *22*, 4229–4240.

Roberts, T.R. (1986). *Danionella translucida*, a new genus and species of cyprinid fish from Burma, one of the smallest living vertebrates. Environ. Biol. Fishes *16*, 231–241.

Ronzitti, E., Ventalon, C., Canepari, M., Forget, B.C., Papagiakoumou, E., and Emiliani, V. (2017). Recent advances in patterned photostimulation for optogenetics. J Opt *11*. https://doi.org/10.1088/2040-8986/aa8299.

Roseberry, T.K., Lee, A.M., Lalive, A.L., Wilbrecht, L., Bonci, A., and Kreitzer, A.C. (2016). Cell-type-specific control of brainstem locomotor circuits by basal Ganglia. Cell *164*, 526–537.

Ryczko, D., and Dubuc, R. (2013). The multifunctional mesencephalic locomotor region. Curr. Pharm. Des. *19*, 4448–4470.

Schneider, C.A., Rasband, W.S., and Eliceiri, K.W. (2012). NIH Image to ImageJ: 25 years of image analysis. Nat Methods *9* (*7*), 671–675. https://doi.org/10.1038/nmeth.2089.

Schulze, L., Henninger, J., Kadobianskyi, M., Chaigne, T., Faustino, A.I., Hakiy, N., Albadri, S., Schuelke, M., Maler, L., Del Bene, F., et al. (2018). Transparent *Danionella translucida* as a genetically tractable vertebrate brain model. Nat. Methods *15*, 977–983.

Seeholzer, L.F., Seppo, M., Stern, D.L., and Ruta, V. (2018). Evolution of a central neural circuit underlies *Drosophila* mate preferences. Nature *559*, 564–569.

Severi, K.E., Portugues, R., Marques, J.C., O'Malley, D.M., Orger, M.B., and Engert, F. (2014). Neural control and modulation of swimming speed in the larval zebrafish. Neuron *83*, 692–707.

Shemesh, O.A., Tanese, D., Zampini, V., Linghu, C., Piatkevich, K., Ronzitti, E., Papagiakoumou, E., Boyden, E.S., and Emiliani, V. (2017). Temporally precise single-cell-resolution optogenetics. Nat Neurosci *20*, 1796–1806. https://doi.org/10.1038/s41593-017-0018-8.

Shukla, R., and Bhat, A. (2017). Morphological divergences and ecological correlates among wild populations of zebrafish (*Danio rerio*). Environ. Biol. Fishes *100*, 251–264.

Thiele, T.R., Donovan, J.C., and Baier, H. (2014). Descending control of swim posture by a midbrain nucleus in zebrafish. Neuron *83*, 679–691.

Watari, N., and Larson, R.G. (2010). The hydrodynamics of a run-and-tumble bacterium propelled by polymorphic helical flagella. Biophys. J. *98*, 12–17.

Weihs, D. (1980). Respiration and depth control as possible reasons for swimming of northern anchovy, *Engraulis mordax*, yolk-sac larvae. Fish. Bull. *78*, 109–117.

Wiggin, T.D., Anderson, T.M., Eian, J., Peck, J.H., and Masino, M.A. (2012). Episodic swimming in the larval zebrafish is generated by a spatially distributed spinal network with modular functional organization. J. Neurophysiol. *108*, 925–934.

STAR★METHODS

KEY RESOURCES TABLE

REAGENT or RESOURCE	SOURCE	IDENTIFIER
Antibodies		
Fab fragments of anti-Fluo-POD	Sigma-Aldrich	Cat#11426346910, RRID: AB_840257
Rabbit GAD65/67 primary antibody	AbCam	Cat# ab11070, RRID: AB_297722
Alexa Fluor 635 secondary antibody goat anti-rabbit IgG	ThermoFisher SCIENTIFIC	Cat#A-31576, RRID:AB_2536186
Bacterial and virus strains		
One Shot™ TOP10 Chemically Competent E. coli	ThermoFisher SCIENTIFIC	Cat#C4040
Biological samples		
Total cDNA *Danio rerio*	This paper	N/A
Total cDNA Danionella cerebrum	This paper	N/A
Chemicals, peptides, and recombinant proteins		
Texas Red dextran (TRD, 3,000 MW, Invitrogen)	ThermoFisher SCIENTIFIC	Cat#D3328
Paraformaldehyde	Electron Microscopy Sciences	Cat#EM-15710, CAS: 30525-89-4
Phosphate Buffered Saline	Euromedex	Cat#EU1-2051-100
Tween 20	VWR	Cat#0777, CAS: 9005-64-5
Methanol	VWR	Cat#8.22283, CAS: 67-56-1
Protease-K	Sigma-Aldrich	Cat#3115887001
Albumin	Sigma-Aldrich	Cat#A4503, CAS: 9048-46-8
Gelatin	Sigma-Aldrich	Cat#G1890, CAS: 9000-70-8
Glutaraldehyde	Sigma-Aldrich	Cat#340855, CAS: 111-30-8
Ethyl-3-aminobenzoate de methanesulfonate (Tricaine)	Sigma-Aldrich	Cat#E10521, CAS: 886-86-2
Critical commercial assays		
PhusionTM High-Fidelity DNA Polymerase	ThermoFisher SCIENTIFIC	Cat#F530
Zero Blunt® TOPO® PCR Cloning Kit	ThermoFisher SCIENTIFIC	Cat#K2800
DIG RNA Labelling Mix	Sigma-Aldrich	Cat#11277073910
Fluorescein RNA Labelling Mix	Sigma-Aldrich	Cat#11685619910
Fluoromount Aqueous Mounting Medium	Sigma-Aldrich	Cat#F4680
Hydrogen peroxide solution	Sigma-Aldrich	Cat#18312, CAS: 7722-84-1
Hydroxyde de potassium	FisherScientific	Cat# 15690800, CAS: 1310-58-3
Tyramide Signal Amplification	Akoya	Cat#FP1498
TSA PLUS FLUORESCEIN	Akoya	Cat#NEL741001KT
Normal Goat Serum	ThermoFisher SCIENTIFIC	Cat#10000C, RRID: AB_2532979
DMSO	Sigma-Aldrich	Cat#D8418, CAS: 67-68-5
N-methyl-D-aspartate (NMDA)	Sigma-Aldrich	Cat#M3262 CAS: 6384-92-5
Experimental models: Organisms/strains		
Danio rerio wildtype	Animal facility of Institut Curie, Paris	N/A
Danio rerio Tg(elavl3:H2B:GCaMP6s)	Animal facility of Institut Curie, Paris	*Tg(elavl3:H2B:GCaMP6s)*
Danio rerio Tg(elavl3:CoChR-eGFP)	Animal facility of Laboratoire Jean Perrin, Paris	*Tg(elavl3:CoChR-eGFP)*
Danionella cerebrum wildtype	Animal facility of Institut Curie, Paris	N/A
Danionella cerebrum Tg(elavl3:H2B:GCaMP6s)	Animal facility of Institut Curie, Paris	*Tg(elavl3:H2B:GCaMP6s)*

(*Continued on next page*)

Continued

REAGENT or RESOURCE	SOURCE	IDENTIFIER
Oligonucleotides		
Primer for *vglut2a* forward: 5′-AGTCGTCTAGCCACAACCTC-3′; reverse: 5′-CACACCATCCCTGACAGAGT-3′	This paper	N/A
Primer for *vglut2b* or *slc17a6b* forward: 5′-GCAATCATCGTAGCCAACTTC-3′ reverse: 5′-ACTCCTCTGTTTTCT CCCATC-3′	This paper	N/A
Primer *for* glyt2 or *slc6a5* forward: 5′-TGGAAGGATGCTGCTACACA-3′ reverse: 5′-TGACCATAAGCCAGCC AAGA-3′	This paper	N/A
Primer for *gad67* or *gad1b* forward: 5′-CCTTCCTCCTCGGCGATTGA-3′ reverse: 5′-GGCTGGTCAGAGAGCTCCAA-3′	This paper	N/A
Recombinant DNA		
Tg(elavl3-H2B:GCaMP6s)	Freeman et al., 2014	Addgene plasmid # 59530
Software and algorithms		
ImageJ	Schneider et al., 2012	https://imagej.nih.gov/ij/
MATLAB 2017b/2019a	MathWorks	N/A
Prism 8/9	GraphPad Software Inc.	N/A

RESOURCE AVAILABILITY

Lead contact

Further information and requests for resources and reagents should be directed to and will be fulfilled by the lead contact, Dr. Filippo Del Bene (filippo.del-bene@inserm.fr).

Materials availability

All unique/stable reagents generated in this study are available from the lead contact without restriction.

Data and code availability

- All data reported in this paper will be shared by the lead contact upon request.
- This paper does not report original code.
- Any additional information required to reanalyze the data reported in this work paper is available from the Lead Contact upon request.

EXPERIMENTAL MODEL AND SUBJECT DETAILS

6 days post-fertilization (dpf) zebrafish (ZF) and *Danionella cerebrum* (DC) larvae (earlier misidentified as *Danionella translucida*) were used for behavioral experiments. At this stage, the larval fish are not sexually mature and the sex is not possible to determine as it is not genetically defined. For imaging experiments, 5 dpf ZF and DC were used. DC adults were grown at a water temperature of 25 to 28°C, pH of 6.3–8.3 and a conductivity of 250–450 uS. Adult DC are fed with Gemma Micro 150 (Skretting, USA) (twice a day) and live *Artemia* (once a day). DC are known to spawn in crevices (Schulze et al., 2018). Hence, 2 to 4 silicone tubes (~5 cm long) were added in the adult tanks to aid spawning.

The larvae were grown at a density of <50 larvae per 90 cm Petri plate in E3 egg medium (without methylene blue). For behavioral experiments, at 5 dpf, both larval ZF and DC were transferred to a 250 mL beaker with 100 mL E3 egg medium (without methylene blue) and fed with rotifers. They were maintained at 28°C in an incubator until the experiment at 6 dpf. The DC larvae were more delicate and required careful handling. Resultantly, the number of DC required to perform each experiment was much larger compared to ZF.

ZF and DC colonies were raised in the animal facility at Institut Curie. The initial DC stocks were procured from Judkewitz lab in Berlin (Schulze et al., 2018). All animal procedures (ZF and DC) were performed in accordance with the animal welfare guidelines

of France and the European Union. Animal experimentations were approved by the committee on ethics of animal experimentation at Institut Curie and Institut de la Vision, Paris.

METHOD DETAILS

Free-swimming behavioral acquisition, fish tracking and tail segmentation

A high-speed camera (MC1362, Mikrotron-GmbH, Germany) and a Schneider apo-Xenoplan 2.0/35 objective (Jos. Schneider Optische Werke GmbH, Germany) were used to carry out the free-swimming acquisitions. The resolution of the images were 800 × 800 pixels with 17 pixels/mm and the acquisition was carried out at 700 Hz. The fish were illuminated with an infrared LED array placed below the swimming arena. An 850 nm infrared bandpass filter (BP850–35.5, Midwest Optical Systems, Inc.) was used on the objective to block all the visible light.

The behavioral arena was illuminated with visible light at 220 lux which was similar to the light intensity in the home incubator. The fish were transferred to Petri plates and acclimatized for >2 h before the behavioral acquisitions. 23 DC and 37 ZF were tested with the acquisition lasting for ∼20–30 min.

Image acquisition, fish tracking and tail segmentation were performed using a custom-written C# (Microsoft, USA) program. The online tracking of the fish and tail segmentation was carried out as described earlier elsewhere (Marques et al., 2018). Briefly, the following method was performed. A background was calculated by taking the mode of a set of frames which are separated in time so that the fish occupies a different position in each frame. This background image was subtracted from each acquired frame. The subtracted image was smoothed using a boxcar filter. A manually selected threshold was used to separate the fish from the background. The fish blob was selected by performing a flood fill starting at the maximum intensity point. The center of mass of this shape was considered the position of the larva. The middle point on a line joining the center of mass of each eye was defined as the larva's head position. The direction of the tail was identified by finding the maximum pixel value on a 0.7 mm diameter circle around the head position. Then, a center of mass was calculated on an arc centered along this direction. The angles of ∼10 tail segments measuring 0.3 mm were calculated. To do this, successive tail segments were identified by analyzing the pixel values along a 120-degree arc from the previous segment. This same algorithm was used for both DC and ZF. The empirically selected threshold to separate the fish from background was different in the two fish.

Analysis pipeline for free-swim data

Poor tracking was identified using pixel intensities of the tail segments. The lost frames, if any, were identified based on a 32-bit timestamp encoded in the first 4 pixels of all the images. These lost frames are then interpolated and filled with NaN values for the recorded parameters.

Discontinuities in turning when the fish turns from 0 to 360° or vice versa were corrected. The raw X and Y coordinates were smoothed using the Savitzky Golay digital filter: in MATLAB (MathWorks, USA), *sgolayfilt* function is used to implement this. A 2nd order polynomial fit was employed on a window size of 21 units (30 ms). Displacement was calculated using these X and Y coordinates of the centroid of the fish.

The measure of tail curvature was used to identify the bouts (Marques et al., 2018). The first 8 tail segments were incorporated in the analysis based on the reliability of the tracking as assessed by the raw pixel intensities. The change in the curvature of the tail was emphasized over local fluctuations by taking a cumulative sum of the values along the tail. The differences in tail angles were calculated as we wanted to detect movements. The tail movements were then smoothed using a boxcar filter of size equivalent to ∼14.30 ms. The absolute of the segment angles were then convolved into a single curvature measure. A maxima/minima filter of 28.6 ms/572 ms was specifically applied to this tail curvature dataset of ZF based on the knowledge of bout and inter-bout durations available to us. An empirically validated cut-off was used on the convolved and smoothed tail curvature measure to identify the starts and ends of swim bouts. It is important to note that in the analysis, only the 'burst' phase of 'burst-and-glide' swims were identified in ZF.

The 7th tail segment was used for calculating tail beat frequency and maximum tail angle. The trace of the tail segment was smoothed and small gaps (less than 7 ms) in the swim events due to tracking were interpolated. Swim events with larger gaps were eliminated from the analysis. Any identified events shorter than 71.5 ms in length, if present, were discarded as well to avoid artefacts. On the bout-based kinematics, the bout distance, inter-bout duration, mean and maximum speed, maximum tail angle and tail beat frequency were calculated.

Half beat based kinematics in ZF and DC

A peak-to-peak half cycle was defined as a half tail beat cycle and this was used for the kinematic calculations to be able to compare a similar unit of locomotion between the two fish.

In ZF: to identify the half-beats, on every swim bout, the absolute of the tail angles was calculated from the 8th segment of the tail and the peaks of tail angle were identified using the *findpeaks* function in MATLAB. Figure S1A shows this for a swim bout in ZF.

In DC: the trace of the tail segment is smoothed using a Savitzky Golay digital filter function of 3rd order with a window size of 50 ms. Small gaps (less than 7 ms) in the tracking were interpolated. Using *bwlabel* function in MATLAB on a binary matrix of good/bad tracking, all continuous stretches of good tracking were labelled. From this, only the stretches longer than 35 frames (or 50 ms)

were selected for further analysis to avoid small tracking artefacts if any. On these identified stretches, half beats were identified as mentioned above for ZF.

On every half beat in both the fishes, the following kinematic parameters were calculated: duration, distance, mean and maximum speed, maximum tail angle and half beat frequency. The 8^{th} tail segment was used for calculating tail beat frequency and max tail angle.

Head-embedded swimming

A high-speed camera (MC4082, Mikrotron-GmbH, Germany) with a Navitar Zoom 7000 macro lens was used to carry out the head-embedded acquisitions. The resolution of the images were 400 × 400 pixels with 75 pixels/mm and the temporal resolution of the acquisition was 100 or 250 Hz. The fish were illuminated with an infrared LED array placed below the swimming arena. An 850 nm infrared bandpass filter (BP850–35.5, Midwest Optical Systems, Inc.) was used on the objective to block all the visible light.

6 dpf DC (n = 4) and ZF (n = 6) were embedded in 0.5 mL of 1.5% agarose. For ZF, nacre incross fish were used. The agarose covered the head up to the pectoral fins. Each fish was acclimatized for at least 90 min before acquisition. Recordings lasted for 10–20 min per fish. The head-embedded videos were primarily used to determine the amount of time spent in swimming. The tail tracking was performed manually to identify the swimming and resting time periods. The duration of swimming was normalized to the total length of the acquisition and reported as a percentage of the total duration of acquisition.

Tap-induced escape behavior

An Arduino controlled solenoid was added to the free-swimming behavioral set-up. The Arduino was triggered from the image acquisition program written in C# (Microsoft, USA). When triggered, the solenoid would hit the surface of the arena from the bottom and cause the fish to escape in response to this stimulus. The trigger was only initiated if the fish was not at the edges of the Petri dish and if there was an inter-stimulus interval of at least 50 s between two consecutive trials. The delay between the trigger onset and the delivery of the solenoid on the arena was estimated and incorporated in the analysis to calculate an accurate reaction time. 19 DC (n = 141 trials) and 15 ZF (n = 159 trials) were tested in the assay. Acquisition at 700 Hz was used for the analysis. However, the illustrated images were captured at 100 Hz.

To analyze the escape kinematics, the peak escape velocities were identified in a window of approx. 450 ms after the stimulus delivery. A peak speed was considered as at least 2 times the peak speed during free-swimming (9.25 mm/s and 42.5 mm/s for DC and ZF, respectively). In case of multiple peak escape velocities in the window, only the first one was considered. Now a 140 ms region of interest was selected around the peak speed to include 40 ms before the peak and 100 ms after the peak as shown in Figure S1K for a ZF. The region of interest was empirically decided after exploring many trials across both the fish species. Mean speed, total distance covered and the delay to reach the peak speed after the stimulus delivery – these parameters were computed for all the trials in each fish. Acceleration was approximated based on the spontaneous and tap-induced swimming kinematics.

The major differences in the processing pipeline from the free-swimming analysis pipeline were as follows. The X/Y displacement vectors were further filtered using a zero-phase digital filtering (*filtfilt* function in MATLAB) with a filter size of 11 ms to identify the peak escape velocities. Kinematics were neither calculated on half beats nor bouts, but on the custom defined 140 ms window for a better comparison of the escape events in the two species of fish.

Mean squared displacement (MSD) and reorientation analysis

Information on X/Y- coordinates was used to compute the Mean squared displacement (MSD) and decorrelation in heading orientation (R) over time. A Savitsky-Golay filter was applied on the X and Y traces to fit a 2^{nd} order polynomial on a 200 ms window. The filtered trajectories were then downsampled to 70 Hz. For each fish, discrete continuous trajectories were identified in a circular region of interest to mitigate border-induced bias. These trajectories were used for the computation.

The time-evolution of MSD and R were calculated at every 100 ms time-step and averaged over all trajectories for each animal. To compute R, we extracted at each time t a unit vector $\mathbf{u}(t)$ aligned along the fish displacement [dx, dy] calculated over a 1s time window. Notice that this vector was only calculated if the fish had moved by at least 0.5 mm in this time period. The heading decorrelation over a period Δt was then computed as $R(\Delta t)=\langle \mathbf{u}(t).\mathbf{u}(t+\Delta t)\rangle_t$. This function R quantifies the heading persistence over a given period: R = 1 corresponds to a perfect maintenance of the heading orientation, whereas R = 0 corresponds to a complete randomization of the orientations. The MSD and R values were plotted over time for DC (n = 23 fish) and ZF (n = 37 fish).

Quantification of depth preference

Three vertical glass cylinders with 36 cm water height were used in this experiment. 6 dpf ZF larvae (n = 30 per cylinder) were added to three cylinders. 6 dpf DC larvae (n = 30 per cylinder) were added to another three cylinders.

The cylinders were considered as consisting of three sections and marked accordingly: the bottom 12 cm, middle 12 cm and the top 12 cm. The number of fish in each section of the column was manually counted once every hour for 10 h. Only the fish that were swimming normally were considered for the enumeration. This was used to calculate the average normalized fish density in every section of the water column.

Quantification of body length and swim bladder inflation

Body length was measured in 5 dpf larvae of the two species (n = 10 for DC and n = 9 for ZF). Pictures of the larvae were captured using an AxioCam MR3 camera. The magnification of the optics was noted and the physical dimension of the camera pixel was used to calculate the pixel size in μm as follows: pixel size = (260/magnification) x binning factor.

To quantify swim bladder inflation, from a population of growing larvae (3 dpf to 15 dpf), five or more larvae were sampled for each age and the proportion of larvae with inflated swim bladder was quantified. The sampling was performed from a growing population of approximately N = 30 DC and 30 ZF. A moving averaging was performed using a window size of two units to smoothen the curve and the swim bladder inflation results were reported from 3.5 to 14.5 days.

Quantification of influence of swim bladder on swimming kinematics in ZF

ZF larvae from 4 to 6 dpf were used and segregated into two groups: larvae with an inflated swim bladder (n = 12) and larvae without an inflated swim bladder (n = 9). Free swimming behavioral acquisitions (15–20 min) were obtained as mentioned before and analyzed for swimming parameters such as total proportion of time spent swimming, bout duration, inter-bout duration and swimming speed. Any fish with less than 10 swim bouts during the acquisition period was not included in the analysis.

Whole-mount *in-situ* hybridization (ISH)

To generate anti-sense probes, DNA fragments were obtained by PCR using Phusion™ High-Fidelity DNA Polymerase (Thermo Scientific™) and the following primers (5'->3') (Kadobianskyi et al., 2019): VGlut2a (forward primer: *AGTCGTCTAGCCACAACCTC*; reverse primer: *CACACCATCCCTGACAGAGT)*, VGlut2b or *slc17a6b* (forward primer: *GCAATCATCGTAGCCAACTTC*; reverse primer: *ACTCCTCTGTTTTCTCCCATC)*, glyt2 or *slc6a5* (forward primer: *TGGAAGGATGCTGCTACACA*; reverse primer: *TGACCA TAAGCCAGCCAAGA)* and gad67 or *gad1b* (forward primer: CCTTCCTCCTCGGCGATTGA; reverse primer: GGCTGGTCAGA GAGCTCCAA). Total cDNA for ZF and DC were used as a template. PCR fragments were cloned into the pCRII-TOPO vector (Invitrogen) according to manufacturer's instructions. All plasmids used were sequenced for confirmation.

Digoxigenin RNA-labeled or Fluorescein RNA-labeled probes were transcribed *in vitro* using the RNA Labeling Kit (Roche Diagnostics Corporation) according to manufacturer's instructions. Dechorionated embryos at the appropriate developmental stages were fixed in fresh 4% paraformaldehyde (PFA) in 1X phosphate buffered saline (pH 7.4) and 0.1% Tween 20 (PBST) for at least 4 h at room temperature or overnight at 4°C. Following this, the samples were preserved in methanol at −20°C until the *in-situ* experiments described below. Whole-mount digoxigenin (DIG) *in-situ* hybridization was performed according to standard protocols (Thisse and Thisse, 2008). A protease-K (10 μg/mL) treatment was performed depending on the age and species of the sample (90 min and 120 min for 5 dpf DC and ZF, respectively). The samples were imaged on a stereoscope with AxioCam MR3 camera.

Vibratome section

The whole-mount samples were embedded in gelatin/albumin with 4% of Glutaraldehyde and sectioned at 20 μm thickness on a vibratome (Leica, VT1000 S vibrating blade microtome). The sections were mounted in Fluoromount Aqueous Mounting Medium (Sigma) before imaging.

Whole-mount fluorescence *in-situ* hybridizations (FISH)

The samples stored in methanol at −20°C were rehydrated by two baths of 50% methanol/PBST followed by two baths of PBST. This was incubated for 10 min in a 3% H_2O_2, 0.5% KOH solution, then rinsed in 50% methanol/50% water and again dehydrated for 2 h in 100% methanol at −20°C. Samples were rehydrated again by a series of methanol baths from 100% to 25% in PBST, and washed two times in PBST. This was followed by an age and species dependent treatment of proteinase K-K (10 μg/mL) at room temperature. At 5 dpf, DC and ZF underwent treatment of proteinase-K for 90 and 120 min, respectively.

Following this, the samples were again fixed in 4% PFA/PBST. After 2 h of pre-hybridization in HY4 buffer at 68°C, hybridization with fluorescein-labelled probes (40 ng probes in 200 μL HY4 buffer) was performed overnight at 68°C with gentle shaking. Embryos were rinsed and blocked in TNB solution (2% blocking solution (Roche) in TNT) for 2 h at room temperature. This was then incubated overnight with Fab fragments of anti-Fluo-POD (Roche) diluted 1:50 in TNB. For signal revelation, embryos were washed with 100 μL Tyramide Signal Amplification (TSA, PerkinElmer) solution and incubated in the dark with Fluorescein (FITC) Fluorophore Tyramide diluted 1:50 in TSA. The signal was then followed for 30 min for *glyt* and 1 h for *vgult2b* until a strong signal was observed. After which, the reactions were stopped by 5 washes with TNT, and incubated for 20 min with 1% H_2O_2 in TNT. All the steps after Fluorescein (FITC) incubation were processed in the dark.

Immuno-histochemistry

Briefly, the whole mount embryos were washed twice in TNT solution. Subsequently, they were blocked for 1 h at room temperature in 10% Normal Goat Serum (Invitrogen) and 1% DMSO in TNT solution. Rabbit GAD65/67 primary antibody (AbCam) diluted 1/5000 in 0.1% blocking solution was incubated overnight at 4°C. The Alexa Fluor 635 secondary antibody goat anti-rabbit IgG (1/500) (Life Technologies) was added in 0.1% blocking solution and incubated overnight at 4°C. After 5 washes in PBST buffer, microscopic analysis was performed.

Confocal imaging of the whole brain FISH/IHC samples

To image the whole brain *in-situ* hybridization and immunohistochemistry samples, we used Zeiss LSM 780, LSM 800 and LSM 880 confocal microscopes with a 10x or 40x objective using appropriate lasers and detection schemes suitable to the labelled sample. Whole brain images were acquired in tiles and stitched together using the stitching algorithm available in Zeiss ZEN blue and ZEN black. The images are shown as maximum intensity projections created on imageJ. In GAD65/67 IHC, non-specific blobs of signal likely originating from residual dye left on the skin after the washing step was removed using image processing in the representative image.

Retrograde labelling of reticulospinal (RS) neurons

A solution containing 10% w/v Texas Red dextran (TRD, 3,000 MW, Invitrogen) in water was pressure injected in the spinal cord (between body segment 7 to 14) of 4dpf ZF and DC. In DC, this method resulted in less efficient labeling of the RS neurons. The best results were obtained by cutting the tail beyond segment 14th with fine scissors and pressure injecting the TRD in the exposed spinal cord. After the labeling, the fish were allowed to recover in E3 egg medium for 24 h at 28°C.

At 5dpf, the surviving injected larvae were anaesthetized with 0.02% Tricaine (MS-222, Sigma), mounted in 1.5% low melting point agarose and imaged under a VIVO 2-photon microscope (3I, Intelligent Imaging Innovations Ltd). Labelling was often sparse and varied among the injected fish which survived to 5dpf (n = 4 fish per species). Maximum intensity projection images of the reticulospinal neurons in ZF and DC is shown from the animals where almost all the RS neurons were labelled. RS neurons in the DC brain were annotated based on their anatomical similarity to the ones in ZF (Kimmel et al., 1982).

Motor activity in spinalized preparation of DC

For spinalization experiments, DC larvae were used at 5–6 dfp (n = 10). Fish were spinalized as already described in McDearmid and Drapeau (2006). Briefly, fish were embedded in 2% agarose with tail-freed and immersed in Ringer's solution containing (in mM): 145 Nacl, 5.4 KCl, 10 HEPES, 1 MgCl2, 1.8 CaCl2 at pH 7.3. Video files were acquired for this experiment. Firstly, a 5–10 min of baseline activity (spontaneous swimming) was recorded. To be sure of a complete rostral spinal lesion, fish heads were completely removed with fine scissors. 5 min of acquisition was recorded after the spinalization step. Following this, 200μL of NMDA (final concentration of 200μM) was added to the fish bath. Another 15 min of recording was obtained in this state. Analysis was carried out manually to calculate the proportion of time spent swimming, duration of swim events and frequency of swim events. In the post-NMDA treatment group, the first 4 min of the acquisition was used to calculate the swimming parameters. In case any fish did not swim during any of the three phases of the acquisition, swim event based kinematics for that specific phase were not calculated.

Generation of pan-neuronal calcium sensor *Tg(elavl3-H2B:GCaMP6s)* line

To generate *Tg(elavl3:H2B-GCaMP6s)* DC fish, 6 ng/μL of the plasmid and 25 ng/μL of Tol2 was used. Injections were performed in embryos which were less than or equal to 4-cell stage. The injection was performed free-hand as DC lay eggs in clutches. Tol2-elavl3-H2B-GCaMP6s plasmid was a gift from Misha Ahrens (Addgene plasmid # 59530; http://n2t.net/addgene:59530; RRID: Addgene_59530) (Freeman et al., 2014).

Light sheet microcopy

Transgenic DC and ZF expressing H2B-GCaMP6s under the *elavl3* promoter were utilized. The GCaMP is nuclear tagged, so its expression is limited to the nucleus which makes it easier for segmentation of the neurons. The fish were embedded in a capillary with 2.5% agar. The tail was freed and recorded simultaneously to extract a readout of the spontaneous swimming behavior. Before each recording, the embedded fish were acclimatized to the recording chamber with the blue laser switched on for at least 10 min. The scanning objective was lateral and the beam entered from the left side of the fish and the detection objective was placed upright on the top. Both the objectives were moved with a piezo so that the light sheets were always in the focal plane of the detection objective. Average laser power was at 0.05 mW. Approximately 280 μm of the brain volume was imaged in each fish. Brain imaging was carried out at approximately 1 Hz (1 whole brain volume/s) and the tail movement was acquired at ∼ 40–80 Hz. Each acquisition lasted for ∼20 min.

Image processing and analysis pipeline for whole-brain light-sheet data

For ZF and DC, image processing was performed offline using MATLAB. Based on visual inspection, if needed, image drift was corrected by calculating the cross-correlation on a manually selected region of interest (ROI). The dx and dy values employed to correct the drift in this ROI were extrapolated to the whole stack. Brain contour was manually outlined on mean greystack images for each layer. Background value for each layer was estimated from the average intensity of pixels outside the brain contour. The segmentation procedure consisted of a regression with a Gaussian regressor convolved with the same Gaussian regressor. The result was regressed another time with the same regressor. Baseline and fluorescence were calculated for each neuron identified by the segmentation. The fluorescence *F(t)* signal was extracted by evaluating the mean intensity across the pixels within each neuron. The tail tracking was performed manually on the tail acquisitions to identify active and inactive time periods. For ZF, the baseline was calculated by the running average of the 10th percentile of the raw data in sliding windows of 50 s. For DC, the baseline for identifying neurons correlated with swim and stop events was calculated as the 10th percentile of the raw

data within each inactive period defined as the time period between 5 s after the end of a swim event and 3 s before the beginning of the next swim event (from tail acquisition data). The baseline values for the active periods were interpolated using the values in the inactive periods. For both ZF and DC, the relative variation of fluorescence intensity *dF/F* was calculated as *dF/F* = (*F(t)* − baseline)/(baseline-background).

For both ZF and DC, neurons from the more rostral part of the brain were removed (y coordinates between y_{max} – 10 um and y_{max}) because of dF/F artefact due to image border. A multi-linear regression was performed using the classical normal equations. In DC, this was performed on dF/F for the whole duration of the experiment and in ZF, on dF/F for a manually selected time period with many well isolated swim bouts. The analysis determines the best-fit coefficient β to explain the neuronal data (y) by the linear combination $y = \sum \beta_j * x_j + \beta_O$, where x_j is the regressor. For ZF, a constant regressor and a swim maintenance regressor (based on the tail acquisition data) were used. For DC, four regressors were used: constant, swim maintenance, swim onset and swim offset. The onset and offset regressors were obtained from the initiation and termination of swim events (based on the tail acquisition data) with a time window of −3 s to +1 s around the initiation/termination event. Swim maintenance, onset and offset regressors were convolved with a single exponential of 3.5 s decay time which approximates the H2B-GCaMP6s response kernel in ZF (Migault et al., 2018). T-scores were computed for every neuron/regressor combination. We could reliably find neurons highly correlated with swim maintenance and termination events as shown in the results.

Brain registration

We used the Computational Morphometry ToolKit CMTK (http://www.nitrc.org/projects/cmtk/) to compute and average the morphing transformation from high resolution brain stacks (184 layers and 1 μm z-resolution; 1-photon imaging) to create a common brain for the *Tg*(*elavl3*:*H2B*:*GCaMP6s*) DC line. All the calcium imaging results were mapped to this reference brain. To compare neuronal populations across different brain samples, we calculated the spatial densities of the considered clusters by using the Kernel Density Estimation (KDE) with a Gaussian kernel with a bandwidth of 12.8 μm. Discrete cluster densities were determined for all points of an inclusive common 3D rectangular grid with an isotropic resolution of 5 μm.

Optogenetic stimulation

5 to 7dpf ZF were head-embedded in a Petri dish with 2% agarose and the tail was freed to move. After a period of acclimatization, fish were placed under a custom made 2-photon (2P) microscope capable of 2P scanning imaging and 2P holographic patterned illumination (Ronzitti et al., 2017). The holographic optical path is analogous to the one described in a previously published work (Accanto et al., 2018). Briefly, the use of fixed phase mask, a diffraction grating and liquid crystal spatial light modulator allows the generation of multiple illumination spots distributed in 3 dimensions (Accanto et al., 2018). Additionally, an inverted compact microscope and an infrared LED (780 nm) were placed below the Petri dish to record the tail movements. 2P scanning imaging of *Tg(elavl3:CoChR-eGFP)* and *Tg(elavl3:H2B-GCaMP6s/6f)* (control) was first performed to locate the MLMN in the midbrain. To target the MLMN population, we defined a holographic illumination pattern composed of multiple identical holographic spots distributed over different x-y-z locations. Each spot has a lateral diameter of 12 μm and an axial FWHM ≈10 μm. On the x-y plane, the targeted surface is covered by the generation of 10 holographic spots, then this pattern is reproduced over 3 different planes to adjust the axial extension of the excitation volume (Figures S4A–S4C). The resulting excitation region corresponds approximately to an ellipsoid of 40-50-70 μm (x-y-z axis, respectively), matching the size of the MLMN in each hemisphere (see Figure 4F). Neurons in these regions were photo-stimulated by 2P excitation with the following protocol: 10 ms pulses at 10 Hz were delivered for 2 s and repeated 3 times with 30 s intervals between repetitions. The effective excitation light intensity varied from 25 to 40 $\mu W/\mu m^2$ and was delivered through a 40x objective (N40X-NIR,0.8 NA,Nikon) by an amplified fiber laser at 1040 nm (Satsuma, Amplitude System), suitable to efficiently excite CoChR opsin (Shemesh et al., 2017). Simultaneous recording of the tail movement was performed on a CMOS camera (MQ013MG-ON Ximea) at a frame rate of 33 Hz. For analysis, the tail tracking was performed manually with the respect to the periods of stimulation. We extracted three swimming parameters during both, spontaneous swimming and stimulation protocol: bout duration, bout frequency and proportion of time spent swimming. The increase or decrease in the mean value of these parameters during the stimulation protocol for each animal is represented in Figure 4H.

QUANTIFICATION AND STATISTICAL ANALYSIS

Behavior data

All the averaged values per fish were prepared in MATLAB 2017b (Mathworks) and statistical tests between the populations were carried out in Prism 8 (GraphPad). Mann-Whitney or Wilcoxon test by ranks was performed as appropriate in all cases where the dataset did not follow a normal distribution.

Light-sheet imaging data

To characterize highly responsive neurons for a specific regressor, the regression coefficient and t-score distributions were first fitted with a Gaussian model (μ_{dist}, σ_{dist}) to estimate a sub-distribution responsible for noise (neurons that do not correlated well with the regressor). These sub-distributions, defined as the maximum distribution ± σ_{dist}, were then fitted again with a Gaussian

model (μ_{nosie}, σ_{noise}). The highly responsive neurons were defined as neurons with both, a regression coefficient higher than regression threshold $_{coefficient} = \mu_{noise\ coefficient} + 3\ \sigma_{noise\ coefficient}$ (or threshold $_{coefficient} = \mu_{noise\ coefficient} + 4\ \sigma_{noise\ coefficient}$) and a t-score higher than t-score threshold $_{t\text{-}score} = \mu_{noise\ t\text{-}score} + 3\ \sigma_{noise\ t\text{-}score}$ (or threshold $_{coefficient} = \mu_{noise\ t\text{-}score} + 4\ \sigma_{noise\ t\text{-}score}$). To quantify the responsiveness of highly correlated neurons, a score was created for each neuron based on the sum of the regression coefficient normalized by the regression threshold$_{coefficient}$ (a_1) and the t-score normalized by the t-score threshold$_{t\text{-}score}$ (a_2). The higher the score, the more responsive is the neuron.